

Journal of Materials Chemistry A

Accepted Manuscript



This is an *Accepted Manuscript*, which has been through the Royal Society of Chemistry peer review process and has been accepted for publication.

Accepted Manuscripts are published online shortly after acceptance, before technical editing, formatting and proof reading. Using this free service, authors can make their results available to the community, in citable form, before we publish the edited article. We will replace this *Accepted Manuscript* with the edited and formatted *Advance Article* as soon as it is available.

You can find more information about *Accepted Manuscripts* in the [Information for Authors](#).

Please note that technical editing may introduce minor changes to the text and/or graphics, which may alter content. The journal's standard [Terms & Conditions](#) and the [Ethical guidelines](#) still apply. In no event shall the Royal Society of Chemistry be held responsible for any errors or omissions in this *Accepted Manuscript* or any consequences arising from the use of any information it contains.

Cite this: DOI: 10.1039/c0xx00000x

www.rsc.org/xxxxxx

ARTICLE TYPE

Solar cells for self-sustainable intelligent packaging

António Vicente,*^a Hugo Águas,^a Tiago Mateus,^a Andreia Araújo,^a Andriy Lyubchuk,^a Simo Siitonen,^b Elvira Fortunato,^a and Rodrigo Martins*^a

Received (in XXX, XXX) Xth XXXXXXXXXX 20XX, Accepted Xth XXXXXXXXXX 20XX

DOI: 10.1039/b000000x

Nowadays there is a strong demand for intelligent packaging to provide comfort, welfare and security to owners, vendors and consumers, by allowing them to know the contents and interact with the goods. This is of particular relevance for low cost, fully disposable and recyclable products like identification tags, medical diagnostic tests, and devices for analysis and/or quality control in food and pharmaceutical industry¹⁻⁴. However, the increase of complexity and processing capacity requires continuous power, which can be addressed by a combined use of a small disposable battery, charged by a disposable solar cell, able to work under indoor lighting. Here, we show a proof-of-concept of the pioneering production of thin-film amorphous silicon (a-Si:H) solar cells with efficiencies of 4%, by plasma enhanced chemical vapour deposition (PECVD), on liquid packaging cardboard (LPC)⁵ commonly used in the food and beverage industry. Such accomplishment put us one step closer to this revolution, by providing a flexible, renewable and extremely cheap autonomous energy packaging system. Moreover, such Si thin films take advantage of their good performance at low-light levels, which also makes them highly desirable for cheap mobile indoor applications.

1. Introduction

Traditional packaging has contributed deeply to increase food and beverage shelf life and to the improvement of the food distribution systems. However, with the increasing complexity of today's society, adding value to packaging has become a priority, namely to address consumer's needs of natural products, with less additives, higher regulation and quality control, to assure food safety, and a fast and optimized distribution process.

Micro- and nano-technologies (MNTs) can be the key to address such demands by imparting the package with the ability to acquire, store and transfer data (smart packaging)⁶ and even to communicate and carry out logic functions to take decisions (intelligent packaging)⁷ and at the same time provide low cost solutions⁸. For this reason, it is estimated that in the next decade nanotechnology will have an impact of 25% on the food packaging market, currently valued at \$100 billion⁹.

The strategy to achieve such impact will involve the production of self-sustained systems that comprise the integration of several functionalities into one single device, such as environmental monitoring⁷, stock tracking¹⁰, package integrity/tampering¹¹ together with features like emissive or reflective digital displays¹² or self-heating or self-cooling packages¹³, which in turn will demand for smart hybridization solutions that combine printed electronics (more cost efficient for large area integration) and silicon technologies (more cost effective per function, such as high-performance communication and advanced processing)¹⁴. Combining printed batteries with a power generator, such as the a-Si:H solar cells described here,

unlocks the spectrum of possible package solutions with incredible added value at a low cost.

The production of solar cells on cellulose-based substrates gained significant importance recently with noteworthy developments¹⁵⁻¹⁹. Its roughness can be advantageous for solar cells as it may contribute to light trapping. On the other hand, it also poses key challenges to practical use, namely cellulose has a relatively low tolerance to temperature and can release some contaminants to both the deposition reactor and the deposited solar cell. Its natural porosity can also favor such release and lower the shunt resistance of the cells (due to short-circuiting). The use of low process temperatures, relative to those (≥ 200 °C) typically employed in processing solar cells with high efficiencies²⁰, is crucial to avoid substrate damage. On the other hand, such challenges are not so crucial for organic solar cells, as they do not require high temperature or vacuum methods. However, their low efficiencies (~2%) and poor environmental stability still pose considerable limitations to the viability of such organic approaches^{16, 21, 22}.

The solar cells developed in this study were produced on packaging cardboard, named "Lunchbox", composed of three layers: 1) the cardboard (with a density of 240 g/m²), consisting on pressed cellulose fibers, which provides mechanical support and resistance to the device, 2) the adhesive layer of low density polyethylene, LDPE (12 g/m²), essential in the lamination process, and 3) the aluminium sheet (6-7 μ m) which serves as

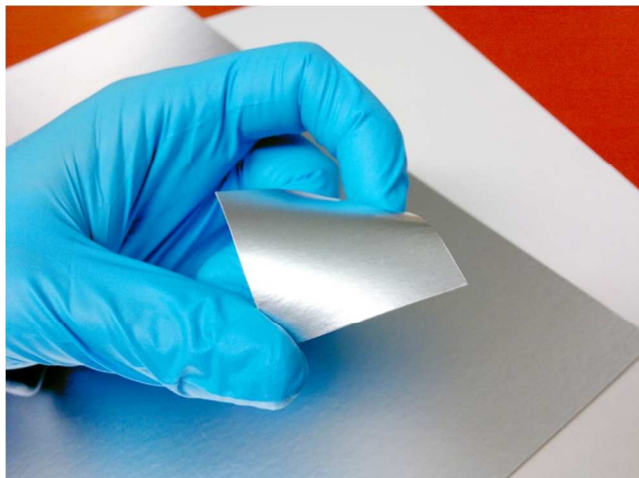


Fig. 1 Picture of the Liquid Packaging Cardboard (LPC) substrate used for a-Si:H solar cell deposition.

rear contact and reflective layer (Fig. 1).

Furthermore, the usage of liquid packaging cardboard (LPC) has environmental advantages, as cellulose comes from sustainable organic sources, hence minimizing the environmental impact of such packages, and industrial advantages since it is compatible with roll-to-roll technology (also the preferred manufacturing process used in packaging industry¹⁴), making it ideal for mass production of solar cells on low cost flexible and disposable substrates for intelligent packaging applications.

2. Experimental details

2.1 Substrate cleaning and characterization.

Reference glass substrates were cleaned sequentially with soap, deionized water, acetone (ultrasonic bath), deionized water and isopropanol (ultrasonic bath). After cleaning, the substrates were dried by N_2 . Liquid packaging cardboards were cleaned solely with a polyester/cellulose blend wiper (which does not leave residues behind) wetted with isopropanol, dried by N_2 and backed at $155\text{ }^\circ\text{C}$ for 12 h.

The LPC surface was analyzed by optical spectroscopy, 3D profilometry and SEM in order to evaluate the metal reflectance, roughness and presence of defects, respectively. Reflectance measurements were obtained in a double beam UV-VIS-NIR Shimadzu spectrophotometer with an integrating sphere. Surface 3D profilometry was performed using an Ambios XP-200 profiler (USA) with a $3\text{ }\mu\text{m}$ line spacing for an area of $3 \times 2\text{ mm}$ and software data compilation from TrueMap. SEM observations were carried out using a Carl Zeiss AURIGA CrossBeam (FIB-SEM) workstation, equipped for EDS measurements. For the FIB experiments, performed to observe the inner cross section of the solar cell, Ga^+ ions were accelerated to 30 kV at 100 pA and the etching depth was kept around 800 nm. A thin layer ($\sim 30\text{ nm}$) of carbon was deposited on the material surface to minimize Ga contamination. Differential scanning calorimetry (DSC) and thermogravimetric analysis (TGA) were carried out in a simultaneous thermal analyser (TGA-DSC-STA 449 F3 Jupiter) at atmospheric pressure. Approximately 7.5 mg of LPC was loaded into an aluminium pan and heated from 40 to $425\text{ }^\circ\text{C}$ with a heating rate of $5\text{ }^\circ\text{C}/\text{min}$.

2.2 Fabrication and characterization of solar cells.

Hydrogenated amorphous silicon (a-Si:H) thin film solar cells were deposited by high frequency (27.12 MHz) plasma enhanced chemical vapour deposition (HRF-PECVD) in a single-chamber reactor, on glass and LPC substrates with $40 \times 40\text{ mm}^2$.

For the reference glass substrate, the first step was the deposition of the Al back contact (200 nm) evaporated in vacuum (10^{-6} mbar) using an e-beam system. The following step, common to both substrates, was the growth of a thin AZO (Al_2O_3 : 2 wt%, ZnO: 98 wt%) layer with $\sim 60\text{ nm}$ deposited by RF-magnetron sputtering, at $155\text{ }^\circ\text{C}$. The AZO resistivity is in the order of $\rho \sim 5 \times 10^{-3}\text{ }\Omega\text{cm}$. The samples were then transferred to the PECVD system where the silicon layers were deposited according to the n-i-p structure. A mixture of SiH_4 and H_2 defines the hydrogen dilution parameter ($D_H(\%) = [H_2/(H_2+SiH_4)] \times 100$). In the case of the intrinsic silicon thin film, $D_H = 80\%$ and the film was deposited at a gas pressure (P_{gas}) of 0.4 Torr and a power density (P_W) equal to $21\text{ mW}/\text{cm}^2$. Adding trimethylboron (TMB, $B(CH_3)_3$) and PH_3 to the mixture of SiH_4 and H_2 produced p- and n-layers, respectively. p-a-Si:H has a $D_H = 92\%$, $R_{\text{TMB}} = \text{TMB}/(\text{TMB}+SiH_4) = 0.68\%$ and was deposited at $P_{\text{gas}} = 1.0\text{ Torr}$, $P_W = 15\text{ mW}/\text{cm}^2$; as for the n-a-Si:H thin film the parameters are: $D_H = 79\%$, $R_{PH_3} = PH_3/(PH_3+SiH_4) = 0.26\%$, $P_{\text{gas}} = 0.4\text{ Torr}$, $P_W = 21\text{ mW}/\text{cm}^2$. More information regarding Si films deposition can be found in supplementary Table S1 and S2.

The electrical properties of the films were studied via temperature dependent dark conductivity, from which the room-temperature conductivity ($\sigma_{d@25^\circ\text{C}}$) and activation energy (E_a) were calculated. The linearity of the $I(V)$ dependence was confirmed before each conductivity measurement. Low voltages (0.1–1 V) were used to reduce high-field effects, such as field-enhanced hopping transport. Coplanar aluminium contacts (200 nm thick, 4 mm long and 1 mm apart) were deposited after the Si active layer by electron beam evaporation.

Lastly, the top-contact IZO (In_2O_3 : 89.3 wt%, ZnO: 10.7 wt%), a transparent conductive oxide with a resistivity in the range of $\rho \sim 5 \times 10^{-4}\text{ }\Omega\text{cm}$, was deposited by RF-magnetron sputtering at room temperature employing a $25 \times 25\text{ mm}$ polyimide mechanical mask with open circles (2.5 mm diameter) to define the cell areas of $\sim 5\text{ mm}^2$.

The solar cells were characterized by current-voltage ($J-V$) measurements at room temperature under AM1.5 ($100\text{ mW}/\text{cm}^2$) light conditions in a Spire Sun Simulator 240A and the external quantum efficiency (EQE) of the cells was determined in short-circuit condition in the wavelength range of 360 to 1100 nm using a home-made set up²³.

Quadrupole Mass Spectroscopy (QMS) real-time process data was collected using a mass spectroscopy system (EXTorr, model XT100M) mounted parallel to the process chamber exhaust line and exhaust gases were collected through a $10\text{ }\mu\text{m}$ sampling orifice located 500 mm away from the outer edge of the RF electrode, for a detection mass range up to 100 amu. Optical Emission Spectroscopy (OES) was used to collect the plasma-emitted light through a photo-collimator placed at a quartz viewport of the reactor (to ensure the recording of total emission of the plasma – from bulk and sheaths) and guided by the optical fiber to an Ocean Optics HR4000 spectrometer with a spectral range of 200–1100 nm.

Cite this: DOI: 10.1039/c0xx00000x

www.rsc.org/xxxxxx

ARTICLE TYPE

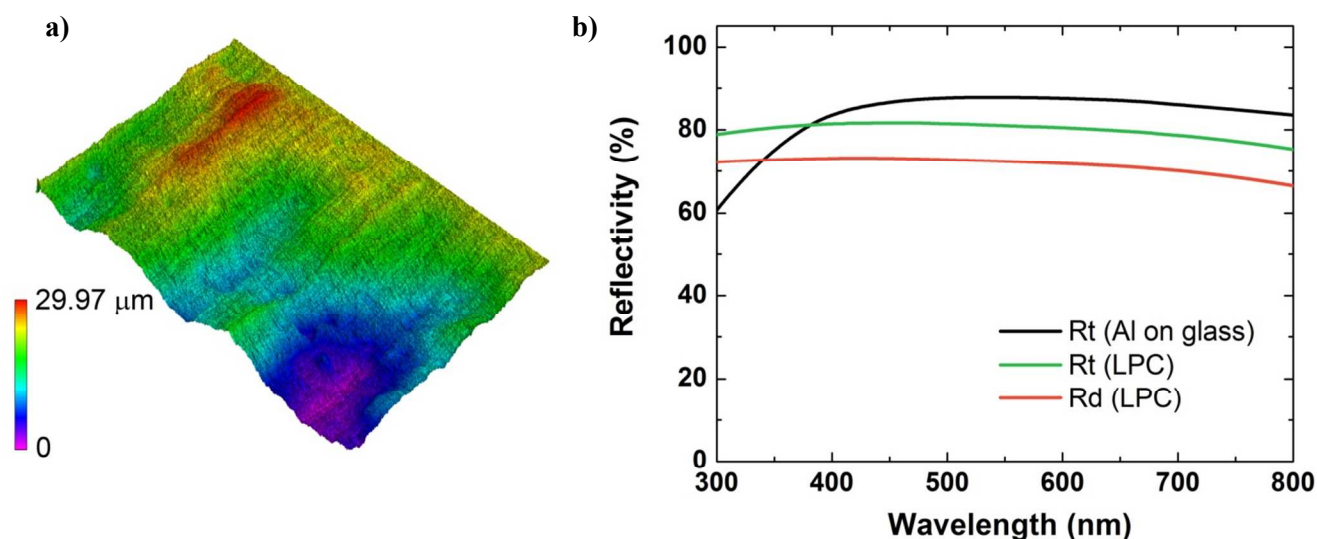


Fig. 2 Surface characterization analysis. (a) 3D profilometer on a 3×2mm area; (b) total (R_t) and diffuse (R_d) reflection in the visible region of LPC and glass coated with aluminium.

3. Results and discussion

The fabrication strategy presented here is able to address the challenges described in the introduction by achieving a good compromise between the deposition conditions, indispensable to obtain an homogeneous coverage of the surface and high quality Si active layers; but also by continuously monitoring the deposition process via Optical Emission Spectroscopy and Mass Quadrupole Spectrometry, tools which control the paper degasification and species present in the deposition chamber. To optimize the cell's layer structure, a fast approach through a design of experiment (DoE) tool was also applied to obtain layers with the adequate thickness and electro-optical characteristics (see Supplementary Fig. S2-S4 and Tables S3-S7).

3.1 Liquid packaging cardboard surface characteristics

Fig. 2, depicts the surface characterization performed on LPC. Fig. 2a, shows that the LPC has a highly rough surface with a root mean square (RMS) value of almost 6 μm . The substrate's reflectivity (Fig. 2b) is around 80% and constant over the entire range of visible spectrum (300 to 800 nm) and the diffuse reflection (R_d) contributes with the biggest fraction to the total reflection (R_t), where $R_t = R_d + R_s$ (specular reflection) and between 300 and 380 nm the total reflection (R_t) is even superior when compared to a 200 nm Al film deposited on glass.

Differential scanning calorimetry was then used to determine the thermal properties of LPC. Fig. 3 depicts the thermogravimetry (TG) and temperature-dependent heat flux (blue dash line) results for laminated cardboard substrate (sample mass: 21 mg). The endothermic peak detected at 99.3 $^{\circ}\text{C}$, with a weight loss of 6.6% ("A" on Fig. 3), indicates the release of

adsorbed water. Due to the low melting temperature of LDPE²⁴, LPC decomposition occurs at 200 $^{\circ}\text{C}$, however up to 250 $^{\circ}\text{C}$ the weight loss is negligible. At temperatures above 250 $^{\circ}\text{C}$, a mass loss of 57.7% ("B" on Fig. 3) occurs, followed by rapid substrate decomposition^{25, 26}. Thus, the substrate is thermally stable up to 200 $^{\circ}\text{C}$ and possibly viable up to 250 $^{\circ}\text{C}$.

Given the intrinsic roughness of the cardboard, coupled with the high reflectivity of the aluminium layer, a surface is free of fissures and its thermal stability at the required low temperature of ~ 150 $^{\circ}\text{C}$, one can be confident of the substrate viability for functional silicon thin film solar cells deposition.

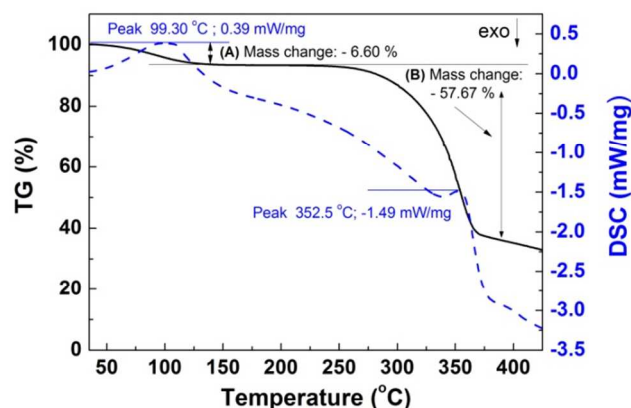


Fig. 3 Temperature-dependent mass change, TG (%), the black line, and heat flux (DSC) signal of cardboard substrate between 40 and 425 $^{\circ}\text{C}$, as the blue dashed line. "A" and "B" identify the two major mass losses.

Cite this: DOI: 10.1039/c0xx00000x

www.rsc.org/xxxxxx

ARTICLE TYPE

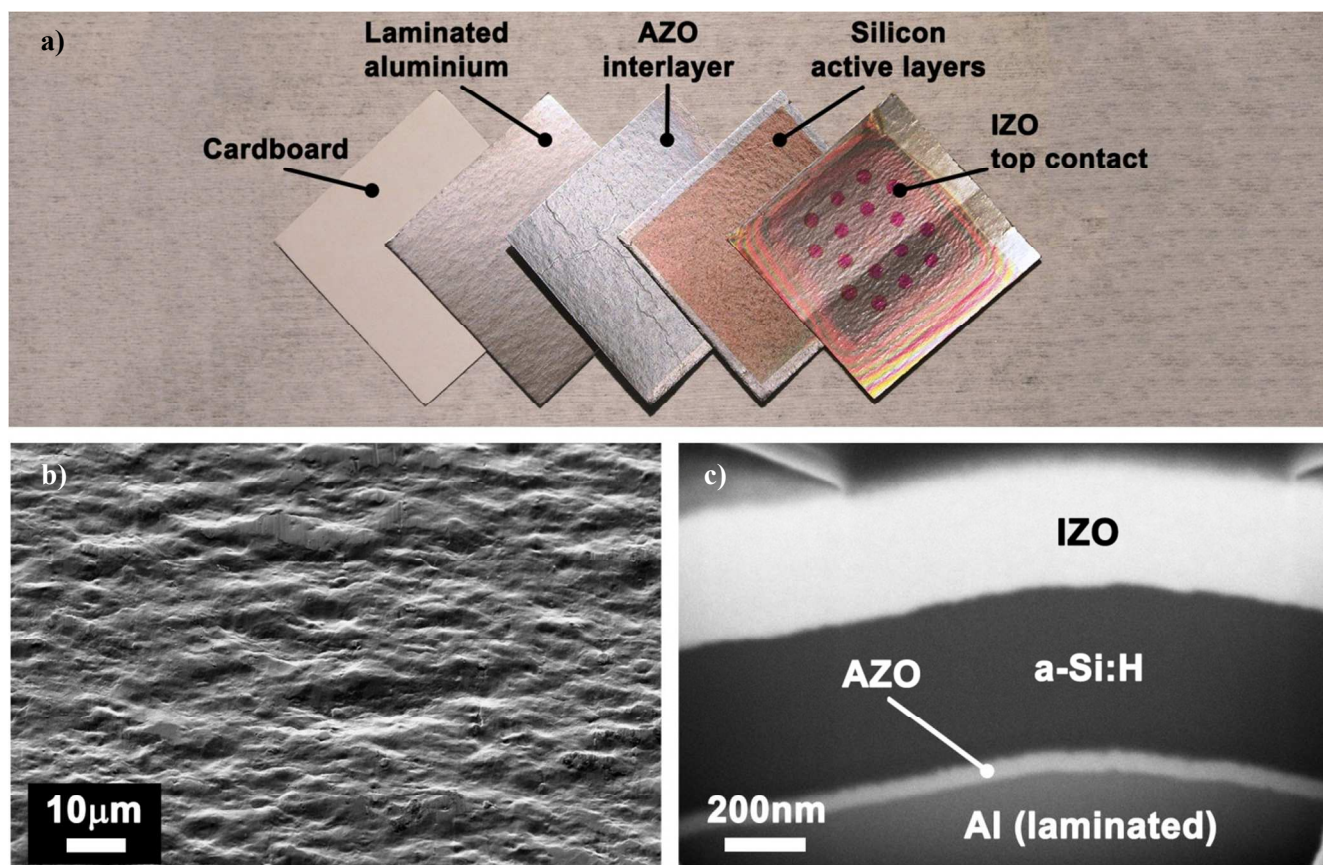


Fig. 4 (a) Photo of the different layers that compose the device chronologically ordered from left to right, starting with the cardboard, the aluminium foil laminated with LPDE which acts as the back contact, the AZO interlayer (~60 nm thickness), the n-i-p silicon layers (~350 nm) and finally the IZO top contact (~300 nm), that also defines the cell area; (b) SEM image of the aluminium surface. One can see a highly rough but free of defects surface; (c) cross-cut FIB image depicting the solar cell layers. The Al (laminated) is a partial cut of the laminated aluminium foil covering the cardboard. The optimized process conditions assure the high conformity of the film to the high substrate roughness and the thickness homogeneity of the layers. The partially peeled layer over the IZO is a protective carbon layer deposited prior to the FIB process to prevent Ga contamination during the etching process.

3.2 The fabrication process of solar cells on liquid packaging cardboard (LPC)

The figure presented next, Fig. 4a highlights the process steps required to produce the solar cells on LPC. Fig. 4b **Error! Reference source not found.** shows highly rough surface but free of cracks and Fig. 4c **Error! Reference source not found.** is a SEM image of the solar cells cross section obtained by FIB showing the quality and homogeneity of the deposited layers.

A critical technical issue concerns the proper selection of the thickness of the solar cell layers in order to achieve the best performance. Starting with non-optimized conditions, a Design of Experiment (DoE) (see Supplementary Fig. S2-S4) study was performed to determine the best combination of layer thicknesses that optimize the solar cell performance. This study led us to select the following thicknesses for the Si layers: n-layer = 30 nm; i-layer = 325 nm; p-layer = 15 nm.

The solar cell deposition process begins with a 60 nm thick

interlayer of AZO deposited at 155 °C, by RF magnetron sputtering, as it contributes for a better optical and electrical matching between the n-layer and the back metal contact and prevents the diffusion of Al impurities to the silicon layers during deposition. It is followed by 3 min hydrogen plasma to assure a surface free of contaminants and reactive species for the subsequent deposition of the silicon layers (see Fig. S5 and Table S8 in Supplementary Information).

To ensure the reproducibility of the cells when switching from glass substrate to LPC, it is required a constant monitoring (by OES and QMS) of the reactive species present in the plasma during silicon layers deposition and general contaminants in the PECVD system.

Concerning the silicon layers, the intrinsic a-Si:H layer has a photosensitivity ($\sigma_{ph}/\sigma_d@25^\circ C$) of 10^7 . The degree of compactness of the thin films and structural order, determined by Spectroscopic Ellipsometry²⁷, led to a high Tauc-Lorentz

parameter (A) of 214, typical of a compact material, and a low broadening term of the *Lorentz Oscillator* (C) of 2.17 which indicates a high short-distance order. These values are typically attributed to i-a-Si:H material with good transport properties and low defect density²⁷. Regarding the doped layers, p-a-Si:H exhibits $\sigma_{d@25^\circ\text{C}} = 1.0 \times 10^{-5}$ S/cm and $E_a = 0.41$ eV, while n-a-Si:H shows $\sigma_{d@25^\circ\text{C}} = 1.9 \times 10^{-2}$ S/cm and $E_a = 0.17$ eV (see Supplementary Table S1 and S2).

Finally, for the top contact, a 300 nm amorphous IZO layer²⁸ was deposited by RF magnetron sputtering at room temperature. IZO has significant advantages, namely its highly smooth surface, with outstanding step coverage, transparency (transmittance above 85% in the visible range) and quite low sheet resistance ($\rho \sim 5 \times 10^{-4}$ Ωcm), for a TCO deposited at room temperature. A mechanical mask was used in order to individualize 16 cells, with an area of ~ 5 mm² each (Fig. 1a). Moreover, cells with larger areas of ~ 20 mm² (see the video in supplementary information) were also produced at an earlier development stage, showing similar efficiencies.

3.2.1 a-Si:H plasma monitoring by OES

Typical thin film deposition processes on conventional substrates (e.g. glass, silicon wafers, etc.) can be performed straightforwardly by repeating a pre-optimized step list, since the properties of their materials remain practically unaltered. However, a well-controlled deposition on organic-based substrates like paper, whose composition can be *a-priori* undetailed and mutate along the process, requires a feedback procedure able to constantly monitor the changes occurring in the substrate and adapt the deposition conditions accordingly. In this section, and in the Supplementary material, we present a set of essential monitoring techniques and the first steps that, according to the authors, are crucial to define a dynamic deposition methodology enabling the reproducible fabrication of solar cells on paper based substrates.

The simplicity of the setup and non-interference with plasma makes OES a useful tool that can provide valuable information about the film forming precursors and radicals present in the plasma²⁹⁻³².

Table 1 presents the intensity peaks ratio of the plasma during the deposition of intrinsic thin film on LPC and Al glass coated. Since, the interpretation of the measured spectra relies on the relative properties of the plasma, the conclusions are drawn from the ratios of two measured intensity emission lines (or peaks), I_x/I_y , where “ I ” refers to the optical emission intensity between the upper and the lower state of transition and “ x ” and “ y ” are the corresponding atoms or molecules (more information can be found in supplementary information Fig. S1).

The identified spectral lines of main interest are the following: Si* ($3s^23p^2 \ ^1D \ 2 \rightarrow \ s^23p4s^1P^0 \ 1$) detected at 288 nm³³, SiH* ($X^2\Pi \rightarrow \ A^2\Delta$ band), detected at 414 nm³³, Balmer H_α ($n = 3 \rightarrow n = 2$) detected at 656 nm³², and H_β ($n = 4 \rightarrow n = 2$), detected at 486 nm³².

It is worth mentioning spectral lines associated with oxygen contaminations, namely oxygen-related transitions can be detected in the spectrum range from 712 to 780 nm³⁴, atomic oxygen spectral lines can be found at 777 and 844 nm, and molecular O_2^* bands at 526, 559, and 599 nm³⁵ and carbon

Table 1 OES peaks ratio under study for the i-, n- and p-type layers deposited on glass (coated with Al or coming glass) and LPC. $I_{H\beta}/I_{H\alpha}$ is the ratio between α and β hydrogen emissions; $I_{H\alpha}/I_{SiH^*}$ ratio between H_α and SiH* optical-emission intensities; I_{Si^*}/I_{SiH^*} intensity ratio of silicon growth precursors Si* and SiH*; I_{O^*}/I_{Si^*} is the ratio between oxygen and silicon optical emission intensities.

Layer	Substrate	Ratio			
		$I_{H\beta}/I_{H\alpha}$	$I_{H\alpha}/I_{SiH^*}$	I_{Si^*}/I_{SiH^*}	I_{O^*}/I_{Si^*}
n-layer	Glass/Al	0.57	0.51	0.176	0.21
	LPC	0.57	0.50	0.175	0.21
i-layer	Corning (200 °C)	0.58	0.61	0.197	0.34
	Corning (145 °C)	0.57	0.56	0.175	0.22
	Glass/Al	0.55	0.58	0.162	0.18
	LPC	0.54	0.59	0.157	0.20
p-layer	Glass/Al	0.90	0.27	0.166	0.16
	LPC	0.91	0.27	0.167	0.15

contamination, such as CH* radiation, detected at 431 nm³⁶. Moreover, to rule out possible contaminations arising from substrate and/or reactor walls and verify the influence of temperature, OES spectra of i-layer deposition was also recorded after reactor cleaning, at 145 and 200 °C, on coming glass.

Regarding possible contaminants, namely carbon and oxygen species, OES is not sensible enough to provide qualitative conclusions. Carbon emission is not observed and oxygen related peaks can be detected, but without significant difference between glass with deposited Al and LPC substrate. As one progresses from the first layer deposited (n-layer) to the last (p-layer), a decrease in the I_{O^*}/I_{Si^*} ratio is observed for all investigated substrates.

Given the fact that H_α and SiH* optical emission intensities indicate the amount of atomic H and growth precursor SiH_n ($n = 1, 2, 3$)³⁷, respectively, thus the ratio $I_{H\alpha}/I_{SiH^*}$ provides a quantitative measure of the relative concentration of atomic H and SiH_n precursors in the plasma³⁸. Though the ratio $I_{H\alpha}/I_{SiH^*}$ does not vary significantly between glass/Al and LPC, in the case of the i-layer deposition over glass at 145 °C, $I_{H\alpha}/I_{SiH^*}$ is slightly lower, which correlates with the higher deposition rate of silicon films grown on glass/Al and LPC substrates. Such variation occurs due to the glass smoothness, where a lower surface area leads to a decrease of the SiH_x precursors' adsorption probability. The intensity of SiH* (I_{SiH^*}) can also be used to infer on the deposition rate as an increase of the SiH* intensity indicates a higher rate³³; such parameter control is essential when producing solar cells³⁹.

The intensity ratios $I_{H\beta}/I_{H\alpha}$ ³⁹⁻⁴¹ and I_{Si^*}/I_{SiH^*} ^{42, 43} also provide information on the electron temperature (Te). Since Te is also sensitive to the gas temperature in the plasma, a higher temperature leads to a decrease of molecular density and elongation of inter-molecular distance for the acceleration of electrons in the plasma and consequently higher Te ⁴⁴. The low deposition temperature of the solar cells (145 °C, below the optimum substrate temperature which is around 200 °C for amorphous silicon⁴⁵), disturbs the balance between the diffusion length of the growth precursors and the hydrogen evolution on the growing. Such facts, allied with the higher roughness of coated glass and LPC, helps to understand why the coming substrate shows a higher intensity ratio.

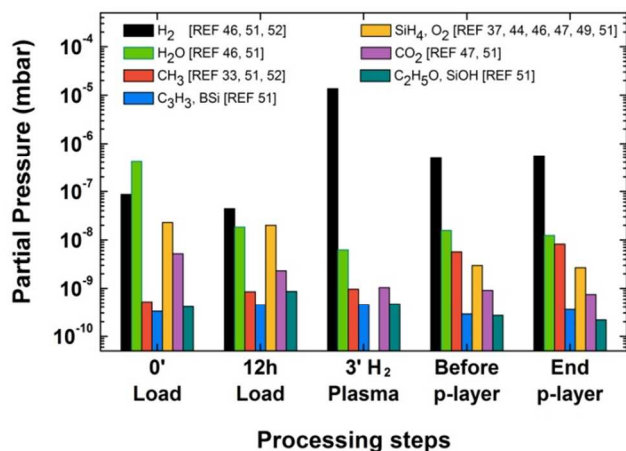
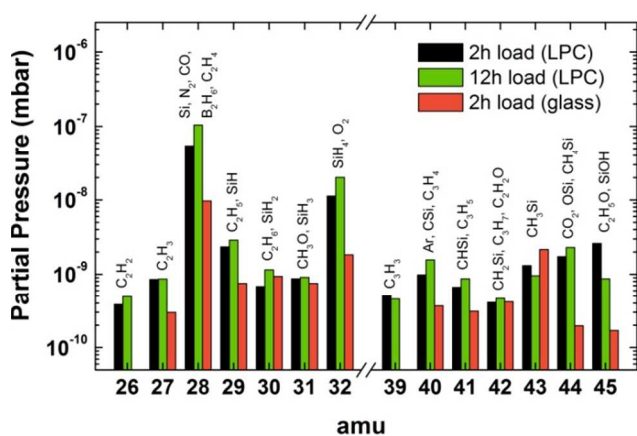


Fig. 5 Partial pressure histograms of the relevant species identified, for different stages of the silicon layers deposition. Namely, immediately after loading the substrate in the PECVD system (0' Load), after 12 h of vacuum pumping and baking at 145 °C (12 h Load), at the end of the initial 3' H₂ cleaning plasma (3' H₂ plasma), before starting the deposition of the p-layer and with stabilized pressure (Before p-layer) and at the end of the p-layer deposition (End p-layer).

3.2.2 MQS monitoring during substrate residence time in PECVD
 10 Quadrupole Mass Spectroscopy (QMS) is a useful tool to analyze plasma since it provides complete information about the gas phase chemical composition. The PECVD production process comprises several steps and, due to the exotic substrate here in study, diverse molecules and contaminants can be present and
 15 contribute differently to the involving atmosphere. Thus, QMS data was collected for depositions on LPC on several stages, described in Fig. 5. For comparison and control, the signal of a glass substrate after 2 h pumping and baking was also collected to establish correlation with possible contaminants present during
 20 solar cell production (Fig. 6). The sum of all the identified peaks partial pressures corresponds to more than 98% of the exhaust gas composition (the complete list of identified species can be found in Supplementary Information (Fig. S6), giving us a realistic overview of the ions/molecules present in the chamber during the
 25 production stages of the solar cell active layers. The remaining 2% are the sum of the relative pressures bellow 10⁻¹⁰ mbar.

The analysis of the solar cell production stages (Fig. 5) shows the importance of vacuum pumping time prior to deposition since it is responsible for the significant reduction of oxygen and water
 30 related species (the partial pressure of such air molecules decreases around 25%). Nevertheless such contaminants are present during the entire process, attesting the large quantities of water adsorbed on the stainless-steel reactor walls⁴⁶ and minute leaks.

35 During pumping, species with higher atomic mass show a constant partial pressure, or even exhibit a small increase. Such increase of species in the mass range of 26-45 amu is related with carboxyl and organic compounds (C_xH_y)⁴⁶⁻⁵¹, arising from cellulose and LDPE due to thermal degradation^{24, 25, 52}. Fig. 6
 40 contributes to the previous statement as one can see that several species after two hours of vacuum pumping and baking, in the case of the LPC, have partial pressure higher when compared to the glass substrate, thus such peaks have a significant contribution of carbon species to the partial pressure. The most



45 Fig. 6 Comparison between LPC and glass substrate partial pressure histograms of the 26-45 amu signals during the pumping and baking (145 °C). For LPC, two instants are depicted: 2 h of vacuum pumping and baking at 145 °C after loading the substrate in the PECVD, in black, and the signals evolution after 12 h of vacuum pumping and baking at 145 °C
 50 (12 h Load), in green. In red is the glass sample under the same baking conditions and by pumping during 2 h.

evident cases are 26 (C₂H₂)^{53, 54}, 28 (N₂, CO, C₂H₄)^{46-50, 53, 54}, 32 (O₂)^{46, 48, 49, 51, 53}, 39 (C₃H₃)⁵³, 44 (CO₂)^{49, 53} and 45 amu
 55 (C₂H₅O)⁵³, which are products of thermal degradation of the cellulose and LDPE^{24, 52, 55}. At low temperature, the thermal degradation of cellulose evolves with dehydration as it leads to depolymerization, and dehydrocellulose^{24, 52} which ultimately yield volatile compounds (carboxyl and carbonyl groups, CO and
 60 CO₂) and char²⁶, also confirmed by the constant contribution of CO₂ to the total pressure after 12h of pumping and throughout the silicon layers deposition.

The fact that the LPC substrate after solar cell deposition become slightly brownish is also indicative that pyrolysis took
 65 place, while LDPE, a thermoplastic made from the monomer ethylene (C₂H₄), produces a wide range of alkanes, alkenes and other species due to the breaking of weak bonds, such as oxygen, incorporated into the main chain as impurities²⁴. Despite the fact that decomposition starts around 200 °C at air atmosphere, here
 70 the polymer is subject to vacuum, hence the solid-liquid phase transition shifts to lower temperatures⁵⁶ leading to such degradation. From Fig. 6 it is also observable the evolution of the amu signals with time (from 2 h to 12 h, for LPC), which shows a slight but clear increase; hence the substrate thermal stability,
 75 under vacuum, is inversely proportional to the pumping time and baking temperature.

On the other hand, peaks that present similar values to the glass substrate (with a stable signal over time) and partial pressure around 10⁻⁹ mbar (where the presence of such organic
 80 molecules is not expected at all) can derive from silicon species degassing from the reactor walls, namely 30 (SiH₂), 31 (SiH₃) and 43 (CH₃Si)⁴⁸. The H₂ plasma reacts with species on the chamber walls and those released due to degassing, hence a decrease in partial pressure for higher mass molecules.
 85 Nonetheless, the consumption of such molecules leads to an increase of lower mass reactive species, as reaction products that will lead to the incorporation of carbon in the AZO/n-a-Si:H interface, thus contributing to the observed decrease in the solar cell current density (J_{SC}), when compared to the same solar cell
 90 deposited on glass (Fig. 7a).

Cite this: DOI: 10.1039/c0xx00000x

www.rsc.org/xxxxxx

ARTICLE TYPE

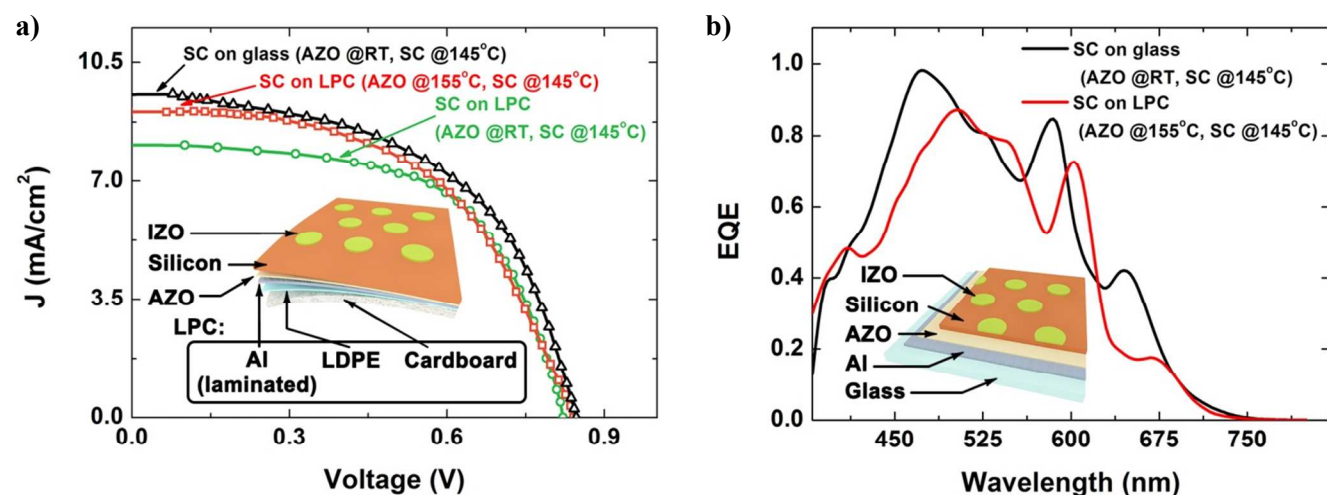


Fig. 7 Performance of a-Si:H solar cells (SCs) deposited on glass and LPC. (a) J - V curves. For the LPC substrate, two different process temperatures were used for the AZO interlayer (room temperature and 155 °C) while the SC Si layers were always deposited at 145 °C. The inset shows the device structure used in this work, wherein the LPC comprises the 3 layers: cardboard, LDPE and laminated Al; (b) External Quantum Efficiency (EQE) of the SC on glass and the best LPC, under the same deposition conditions. The inset shows the glass reference device structure.

3.2.3 Solar cell characterization

Taking into consideration the physical and thermal effects which the deposition process has on the LPC, it was possible to achieve a good compromise between, low temperature, gas flows, power density and growth rate to obtain homogeneous layers, and through a extensive analysis of plasma monitoring, to assure reproducibility of the characteristics of the layers, namely thickness, electro and optical properties.

With the deposition process optimized, the best initial value for the a-Si:H solar cells on LPC has 4.08% efficiency, FF = 53.7%, J_{SC} = 9.05 mA/cm² and V_{OC} = 0.84 V (Fig. 7 and Table 2). It is worth noting that the deposition of the AZO interlayer at a high temperature (155 °C) improves considerably the solar cells, leading to a performance similar to the cells on conventional glass substrates. This can be attributed to the temperature-induced high-strain stresses on the substrate during the deposition processes⁵⁷, namely the LDPE loses its rigidity when subjected to \approx 100 °C temperature and, together with vacuum, makes the

Table 2 Comparison of the solar cell properties deposited on glass and LPC substrates; η , efficiency; FF, fill factor; J_{SC} , short-circuit current density; V_{OC} , open-circuit voltage.

Solar cell (substrate)	η (%)	FF (%)	V_{OC} (V)	J_{SC} (mA/cm ²)	R_S (Ω cm)	R_{Sh} (Ω cm)
LPC (AZO @RT)	3.98	60.1	0.82	8.08	23	984
LPC (AZO @155 °C)	4.08	53.7	0.84	9.05	31	831
Glass (AZO @RT)	4.33	53.3	0.85	9.55	21	446

laminated aluminium crease. Thus, by allowing this conformation to take place before the silicon layers deposition, the mechanical deformations are lower and the mismatch between thermal expansion coefficients of the substrate and film decrease⁵⁷.

The external quantum efficiency (EQE) measurements depicted in Fig. 7b, for solar cells on glass and the LPC show that the main portion of the photocurrent is produced in the wavelength range between 450 and 550 nm. Above 550 nm the light traverses the Si layers and is reflected back to the cell by the Al rear contact, thereby forming interference within the thin Si film which gives rise to the EQE peaks observed in the longer wavelength region (550 – 800 nm)⁵⁸.

Furthermore, the number of working cells attained in this substrate is similar to the one on glass, near 100%, over the working area of 25 × 25 mm. However, LPC is flexible and the solar cells can resist some degree of paper bending (radius of \sim 5 mm) with a minimal effect on their performance, \sim 2% variation of the initial value, which evidences the suitability of LPC as a substrate for a-Si:H cell deposition. The resistance of inorganic TCOs and a-Si:H on flexible substrates (cellulose⁵⁹ and polymeric substrates⁶⁰) has been previously demonstrated with films deposited under similar conditions and techniques; showing excellent electrical performances even at a bending radius of 5 mm for TFTs⁶¹ and 20 mm for a-Si:H PV modules over more than 800 bending cycles⁶⁰.

Certain process-related factors have limited the efficiencies attained in this work (\sim 4%), reported in Table 2. Namely, the low production temperature and possible cross contamination

Cite this: DOI: 10.1039/c0xx00000x

www.rsc.org/xxxxxx

ARTICLE TYPE

Table 3 Material cost distribution of a-Si:H solar modules on LPC, PEN/PET, stainless steel and flexible glass per square meter (cost, \$ per m²). “Low” column relates to an optimum estimative, while the “High” column considers the upper limit of the price range.

Cost component	LPC		PEN/PET		Stainless steel		Flexible glass		
	Low	High	Low	High	Low	High	Low	High	
Antireflection layer	1.2 ^a	6.0 ^a	1.0	5.0	1.0	5.0	1.0	5.0	
Top contact (TCO)	2.0	5.0	2.0	5.0	2.0	5.0	2.0	5.0	
Bottom contact (metal/TCO)	N/A ^b	N/A ^b	2.0	5.0	N/A	N/A	2.0	5.0	
Electrical contacts and interconnects	2.9	6.0	2.9	6.0	2.9	6.0	2.9	6.0	
Encapsulant	0.1 ^c	4.4 ^d	2.9	4.4	2.9	4.4	1.9	5.5	
Sealant	0.1	4.4	2.9	4.4	2.9	4.4	3.6	5.4	
Thin Film Si ^e	Material	2.0	30.0	2.0	30.0	2.0	30.0	2.0	30.0
	Energy	1.8 ^f	6.0 ^f	1.5	5.0	1.5	5.0	1.5	5.0
	Process	3.0 ^f	14.4 ^f	2.5	12	2.5	12.0	2.5	12.0
	Maintenance	1.8 ^f	4.8 ^f	1.5	4.0	1.5	4.0	1.5	4.0
Effective total	14.9	81.0	21.2	80.8	19.2	75.8	20.9	82.9	
Substrate	0.5 ^g	0.8 ^h	5.0 ⁱ	8.0 ^j	4.0 ^k	4.0	7.5 ^l	20.0	
Total	15.4	81.8	26.2	88.8	23.2	79.8	28.4	102.9	

^a An extra cost of 20% is considered since the deposition process requires temperature to assure proper degassing and decrease adhesion stress.

^b Not Applied. The LPC and stainless steel substrates already encompasses the bottom contact.

^c Estimated from the substrate industrial cost. Considering the composition fractions of the total substrate, LDPE accounts for 20%, which provides a rough estimation of the encapsulation cost.

^d Considering the high cost for encapsulating a flexible SC (plastic substrate).

^e High end price also considers increase in cost in the case of a double junction solar cell.

^f The costs were increased by 20% due to higher consumption of energy, processing and maintenance when compared with other substrates, resulting from the increased pumping time and reactor cleaning.

^g Value provided by the packaging industry; ^h Value estimated for the end-user; ⁱ Kalowekano *et al.* (2009)⁶²; ^j Krebs *et al.* (2010)⁶³; ^k Brown *et al.* (2014)⁶⁴.

^l Value estimated from industrial glass⁶⁵ plus 25% to compensate handling, transportation and usage, since flexible glass is highly susceptible to breaking and cracking along the edges if even slightly mishandled.

15 due to the Si deposition in a single PECVD chamber, as opposed to a multi-chamber system, which could lead to improvements above 30%. Nevertheless, the solar cells performance on standard glass and on LPC is demonstrated to be remarkably similar. The slightly lower efficiency of the cells deposited on LPC is
20 expected, since for flexible substrates the deformation induces an accumulation of mechanical stresses (compressive and tensile), which lead to a higher defect density⁶⁶.

Concerning the estimated devices durability, given the type of indoor applications and the expected time frame of utilization
25 around one year, for a-Si:H cells deposited on the onset of crystallinity and with comparable ratio $R = \text{H}_2/\text{SiH}_4 = 4$, the degradation after 1000h under 3000 lx (1 mW/cm²) of a typical indoor spectrum of a F12 fluorescent lamp (with significant UV component) is less than 10%⁶⁰. The devices analysed in this work
30 have been able to endure indoor environmental conditions for a prolonged time and after 14 months they still show comparable

efficiencies. Therefore, such light-induced degradation is not expected to hinder their application in low cost sustainable commodities. Moreover, a-Si:H cells have the advantage of a
35 high absorption coefficient (10^4 - 10^5 cm⁻¹) in the visible range and can absorb diffused light, which means that these cells are capable of generating voltages close to their characteristic V_{OC} under typical indoor ambient light conditions⁶⁷.

To better understand the applicability of these solar cells on
40 LPC, it can be compared with the power generated by a commercial printed battery, as that of Enfucell, which already has a wide range of applications from transdermal delivery patches to wireless – BLE – sensor tags⁶⁸. The SoftBattery Reg 1,5V (Plus) from Enfucell can supply 1.5 V

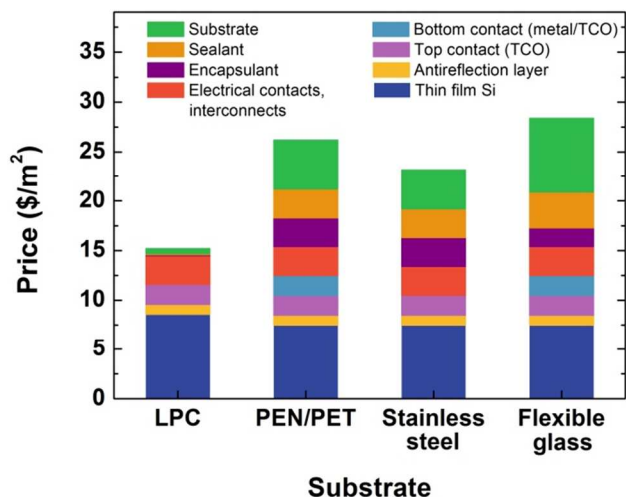


Fig. 8 Manufacturing cost (\$/m²) comparison between LPC, PEN/PET, stainless steel and flexible glass.

and 8-10 mA on an area of 60 × 72 mm. With the proof of concept solar cells presented here, it is possible to achieve a similar output, over an area of 30 × 20 mm, by arranging two rows, each with three cells in series, connected in parallel. This arrangement can output ~2 V and ~15 mA, which shows the potential impact of the devices developed in this work.

4. Cost estimation of industrial manufacturing of solar cell on packaging cardboard

Assessing the economic viability of LPC as a solar cell substrate for indoors applications helps to put in perspective its relevance and understand why it is important to tackle the emerging field for intelligent packaging and low power disposable consumer electronics. One of the foremost advantages is the fact that the infrastructure and equipment involved in the production of these devices not only matches that commonly used today in 2nd generation solar cell production, but it is also compatible with roll-to-roll technology⁶⁹ which is the preferred manufacturing process in packaging industry. Thus, no extra major capital expenses in terms of manufacturing equipment are required.

To perform the cost-effectiveness analysis presented next (Table 3 and Fig. 8), LPC is compared with three other viable substrates for flexible solar cells, namely PEN/PET, stainless steel⁶⁴ and a recent technology, flexible glass⁷⁰. Two assumptions are made, in addition to the inexistence of extra capital cost for the construction/adaptation of a production unit, which are: 1. Since only the production process is being considered and not the end user applications, the calculations will be done solely for the solar cell production and not for the process that comes after the solar cell deposition (namely, mounting, wiring, equipment and other capital costs). This way one can highlight the influence arising from the substrate in the final expenditure; 2. Regarding encapsulation, paper based solar cells, besides the typical encapsulation process used in flexible solar cell for higher protection, LPC can undergo a cheaper one considering the final LDPE protective layer applied in the cardboard packaging industry.

Table 3 describes all the costs (\$/m²) related to material and processes for a low/optimum estimated cost and possible high

end of price range. Price estimations and calculations are presented elsewhere⁶⁵, unless described otherwise. Electricity generated as \$/Wp is calculated by dividing the manufacturing cost (\$/m²) by the output of the same area (1000 Wp/m²) times efficiency. Assuming a module efficiency equal to the present 4% solar cell efficiency, the manufacturing cost will be between \$0.38/Wp, for the optimum price estimative, and \$2.04/Wp for the case of an estimation of the upper price range. Fig. 8 helps to visualize the material cost distribution, for the lower estimated values, and compare the impact that the different substrates have in the final value. Since LPC has the lowest substrate cost, the manufacturing cost is significantly reduced, besides the considered 20% higher silicon thin film process cost.

Considering the cost of paper-based PV, the LPC falls in an economically viable price range. However, even assuming a small increase in efficiency up to 5%, which *Brinza et al* were able to achieve for 100 °C on stainless steel foil⁷¹, and assuming a module efficiency equal to the cell efficiency, the manufacturing cost will drastically reduce to \$0.31-\$1.64/Wp (optimum and high estimative, respectively), giving LPC a competitive price for low cost PV.

5. Sustainability and recyclability of solar cells on packaging cardboard

Regarding the recyclability of solar cells on LPC substrates, the cardboard packaging industry already has a mature recycling process⁷², briefly, it consists in mixing the packaging cardboard with water; the wood fibres separate from LDPE and aluminium, allowing paper pulp to be reused and the mixture LDPE/Al to be turned into new products⁷³. The added value that a solar cell can bring will not hinder that fact, since the quantity of active semiconductor material in the cell is extremely small. In fact, recently, paper mills are also applying pyrolysis to separate the LDPE and Al (poly-al) by heating up to 500 °C, without oxygen. This way, the plastics do not burn and the evaporated gas by-product is used to generate electricity and steam, and the resulting Al has a high-grade purity⁷⁴.

Concerning the solar cell material, the a-Si:H has a suitable relation in terms of environmental impact vs. production cost⁷⁵ compared with most photovoltaic materials. The pay-off time for the present devices is estimated to be in the range of 0.4 – 2 years, assuming large-scale roll-to-roll manufacturing processes, which is comparable to the lifetime of several disposable packaging applications.

6. Conclusions and challenges for future development

In the present study, it is demonstrated for the first time, to the authors' knowledge, the viability of fabricating a-Si:H solar cells at low temperature, with efficiencies of 4%, on liquid packaging cardboards, which naturally incorporate a high quality Al back contact compatible with the silicon thin film deposition conditions by PECVD. A working device can be seen in the Supplementary Video. The potential of our technology could only be attained after proper improvement of the process parameters, such as a special control of the process gas dilution, the systematic study of doping from gas phase⁷⁶, hydrogen plasma treatment (see Supplementary Fig. S5) and the fabrication of n-i-p

junctions and contacts with the adequate layer thicknesses and electro-optical characteristics^{77, 78}; together with studies devoted to process monitoring and interface quality improvement, which proved to be highly relevant.

We also identified engineering challenges to improve the device efficiency and throughput that require the use of multi-chamber systems (to avoid cross contaminations and enhance the throughput) and by using effective light trapping schemes, as those based on scattering nanoparticles⁷⁹. Further research is also needed in how to improve the LPC integrity, by optimizing the lamination polymer, LDPE, to seal the cellulose and prevent the loss of water inside the LPC, crucial to preserve its intrinsic flexibility and counteract the fragility that the production process can cause on the substrate⁶¹. Finally, the optimization of the cell production will also address the utilization of In free front TCO. As a critical material, the use of In should not be applied in disposable and low cost applications; nevertheless the process must be performed at room temperature and exhibit similar performances as on-going work points out⁸⁰.

The innovation reported here is a significant step towards an energetic revolution of mobile and intelligent systems, by opening the path for several new solar cells applications in low cost disposable products. This can produce a tremendous impact on today's existing smart packaging industry and promote spin-offs towards other relevant fields of mobile systems, disposable electronics and smart textiles.

Acknowledgements

This work was funded by the Portuguese Science Foundation (FCT-MEC) through the projects EXCL/CTM-NAN/0201/2012, Strategic Project PEst-C/CTM/LA0025/2013-14 and A3Ple (FP7, NMP-2010-SME-4 grant 262782). Moreover, this work was also supported by E.F.'s ERC 2008 Advanced Grant (INVISIBLE contract number 228144).

The authors want to thank their colleagues Daniela Gomes for SEM images acquisition, Rita Branquinho for helping with 3D profilometer, Alexandra Gonçalves for STA measurements and Manuel J. Mendes for revising the manuscript.

A.V. acknowledges the support from the Portuguese Foundation for Science and Technology (FCT) and MIT-Portugal through the scholarship SFRH/BD/33978/2009.

Notes and references

^a CENIMAT/I3N, Departamento de Ciência dos Materiais, Faculdade de Ciências e Tecnologia, FCT, Universidade Nova de Lisboa and CEMOP/UNINOVA, 2829-516 Caparica, Portugal. Fax: +351 212941365; Tel: +351 212948525; E-mail: amv17109@campus.fct.unl.pt; rm@uminova.pt

^b Stora Enso Oyj, Renewable Packaging, Research Centre Imatra, Tornansaarenraitti 48, 55400 Imatra, Finland

† Electronic Supplementary Information (ESI) available: [Experimental details and preliminary results: Fabrication and characterization of silicon thin films; Liquid packaging cardboard surface analysis: Optical Emission Spectroscopy (OES); Design of Experiment and mathematical modeling (DoE); Influence on the solar cell properties of performing hydrogen plasma treatment on the substrate; Quadrupole Mass Spectroscopy (QMS)].

1. D. Tobjork and R. Osterbacka, *Advanced Materials*, 2011, 23, 1935-1961.

2. M. Berggren, D. Nilsson and N. D. Robinson, *Nat. Mater.*, 2007, 6, 3-5.
3. Y. G. Sun and J. A. Rogers, *Advanced Materials*, 2007, 19, 1897-1916.
4. R. Martins, I. Ferreira and E. Fortunato, *Physica Status Solidi-Rapid Research Letters*, 2011, 5, 332-335.
5. Stora Enso, <http://www.storaenso.com/>.
6. R. F. P. Martins, A. Ahnood, N. Correia, L. Pereira, R. Barros, P. Barquinha, R. Costa, I. M. M. Ferreira, A. Nathan and E. Fortunato, *Advanced Functional Materials*, 2013, 23, 2153-2161.
7. K. L. Yam, P. T. Takhistov and J. Miltz, *Journal of Food Science*, 2005, 70, R1-R10.
8. N. Sozer and J. L. Kokini, *Trends in Biotechnology*, 2009, 27, 82-89.
9. C. M. Lopes, J. R. Fernandes and P. Martins-Lopes, *Food Technology & Biotechnology*, 2013, 51, 183-197.
10. R. J. Lehmann, R. Reiche and G. Schiefer, *Computers and Electronics in Agriculture*, 2012, 89, 158-174.
11. D. A. Pereira de Abreu, J. M. Cruz and P. Paseiro Losada, *Food Reviews International*, 2011, 28, 146-187.
12. A. P. F. Turner, *Chem. Soc. Rev.*, 2013, 42, 3184-3196.
13. N. P. Mahalik and A. N. Nambiar, *Trends in Food Science & Technology*, 2010, 21, 117-128.
14. H. E. Nilsson, T. Unander, J. Siden, H. Andersson, A. Manuilskiy, M. Hummelgard and M. Gulliksson, *Ieee Transactions on Components Packaging and Manufacturing Technology*, 2012, 2, 1723-1734.
15. M. C. Barr, J. A. Rowehl, R. R. Lunt, J. Xu, A. Wang, C. M. Boyce, S. G. Im, V. Bulovic and K. K. Gleason, *Advanced Materials*, 2011, 23, 3500-+.
16. Y. H. Zhou, C. Fuentes-Hernandez, T. M. Khan, J. C. Liu, J. Hsu, J. W. Shim, A. Dindar, J. P. Youngblood, R. J. Moon and B. Kippelen, *Scientific Reports*, 2013, 3.
17. M. L. Brongersma, Y. Cui and S. Fan, *Nat Mater*, 2014, 13, 451-460.
18. Z. Fan, H. Razavi, J.-w. Do, A. Moriwaki, O. Ergen, Y.-L. Chueh, P. W. Leu, J. C. Ho, T. Takahashi, L. A. Reichertz, S. Neale, K. Yu, M. Wu, J. W. Ager and A. Javey, *Nat Mater*, 2009, 8, 648-653.
19. M. Kaltenbrunner, T. Sekitani, J. Reeder, T. Yokota, K. Kuribara, T. Tokuhara, M. Drack, R. Schwodiauer, I. Graz, S. Bauer-Gogonea, S. Bauer and T. Someya, *Nature*, 2013, 499, 458-+.
20. M. Stuckelberger, Y. Riesen, M. Despeisse, J.-W. Schüttauf, F.-J. Haug and C. Ballif, *Journal of Applied Physics*, 2014, 116, -.
21. M. C. Barr, J. A. Rowehl, R. R. Lunt, J. J. Xu, A. N. Wang, C. M. Boyce, S. G. Im, V. Bulovic and K. K. Gleason, *Advanced Materials*, 2011, 23, 3500-+.
22. S. Roy, R. Bajpai, A. K. Jena, P. Kumar, N. kulshrestha and D. S. Misra, *Energy & Environmental Science*, 2012, 5, 7001-7006.
23. S. Morawiec, M. J. Mendes, S. A. Filonovich, T. Mateus, S. Mirabella, H. Águas, I. Ferreira, F. Simone, E. Fortunato, R. Martins, F. Priolo and I. Crupi, *Optics Express*, 2014, 22, A1059-A1070.
24. S. o. F. P. E. National Fire Protection Association, *SFPE handbook of fire protection engineering*, National Fire Protection Association ; Society of Fire Protection Engineers, Quincy, Mass.; Boston, Mass., 1995.

25. T. Andersson, B. Stålbom and B. Wesslén, *Journal of Applied Polymer Science*, 2004, 91, 1525-1537.
26. F. Shafizadeh, *Abstracts of Papers of the American Chemical Society*, 1983, 186, 75-FUEL.
27. H. Águas, V. Silva, E. Fortunato, S. Lebib, P. R. i. Cabarrocas, I. Ferreira, L. Guimarães and R. Martins, *Japanese Journal of Applied Physics*, 2003, 42, 4935.
28. P. Barquinha, G. Goncalves, L. Pereira, R. Martins and E. Fortunato, *Thin Solid Films*, 2007, 515, 8450-8454.
29. S. Muthmann and A. Gordijn, *Solar Energy Materials and Solar Cells*, 2011, 95, 573-578.
30. J. K. Rath, M. Brinza, Y. Liu, A. Borreman and R. E. I. Schropp, *Solar Energy Materials and Solar Cells*, 2010, 94, 1534-1541.
31. L. Shui-Yang, C. Yu-Cheng, C. Yun-Shao, C. Yin-Yu and L. Shuo-Jen, *Electron Devices, IEEE Transactions on*, 2012, 59, 1245-1254.
32. B. Strahm, A. Feltrin, R. Bartlome and C. Ballif, 2009, 74090E-74090E.
33. S.-Y. Lien, Y.-Y. Chang, Y.-S. Cho, J.-H. Wang, K.-W. Weng, C.-H. Chao and C.-F. Chen, *Journal of Non-Crystalline Solids*, 2011, 357, 161-164.
34. G.-F. Hou, X.-H. Geng, X.-D. Zhang, J. Sun, J.-J. Zhang and Y. Zhao, *Chinese Physics B*, 2011, 20.
35. E. Vassallo, A. Cremona, F. Ghezzi and D. Ricci, *Vacuum*, 2010, 84, 902-906.
36. K. Tsuji and K. Hirokawa, *Thin Solid Films*, 1991, 205, 6-12.
37. J. Ge, Z. P. Ling, J. Wong, R. Stangl, A. G. Aberle and T. Mueller, *Journal of Applied Physics*, 2013, 113, -.
38. Z. M. Wu, J. Sun, Q. S. Lei, Y. Zhao, X. H. Geng and J. P. Xi, *Physica E-Low-Dimensional Systems & Nanostructures*, 2006, 33, 125-129.
39. J. K. Rath, A. D. Verkerk, Y. Liu, M. Brinza, W. J. Goedheer and R. E. I. Schropp, *Materials Science and Engineering B-Advanced Functional Solid-State Materials*, 2009, 159-60, 38-43.
40. Y. Liu, A. D. Verkerk, J. K. Rath, R. E. I. Schropp and W. J. Goedheer, in *Physica Status Solidi C - Current Topics in Solid State Physics, Vol 7 No 3-4*, ed. R. E. I. Schropp, 2010, vol. 7, pp. 575-578.
41. K. Saito and M. Kondo, *Physica Status Solidi a-Applications and Materials Science*, 2010, 207, 535-538.
42. Y.-S. Lee, J.-H. In, S.-K. Ahn, S.-H. Seo, H.-Y. Chang, D.-J. You, S.-W. Ahn and H.-M. Lee, *Current Applied Physics*, 2010, 10, S234-S236.
43. M. Takai, T. Nishimoto, M. Kondo and A. Matsuda, *Science and Technology of Advanced Materials*, 2001, 2, 495-503.
44. Y. Sobajima, T. Higuchi, J. Chantana, T. Toyama, C. Sada, A. Matsuda and H. Okamoto, in *Physica Status Solidi C - Current Topics in Solid State Physics, Vol 7 No 3-4*, ed. R. E. I. Schropp, 2010, vol. 7, pp. 521-524.
45. A. Matsuda, *Japanese Journal of Applied Physics Part 1-Regular Papers Short Notes & Review Papers*, 2004, 43, 7909-7920.
46. H. A. Weakliem, R. D. Estes and P. A. Longeway, *Journal of Vacuum Science & Technology A*, 1987, 5, 29-36.
47. A. I. Chowdhury, T. M. Klein, T. M. Anderson and G. N. Parsons, *Journal of Vacuum Science & Technology A*, 1998, 16, 1852-1856.
48. O. Gabriel, S. Kirner, M. Klick, B. Stannowski and R. Schlatmann, *EPJ Photovolt.*, 2014, 5, 55202.
49. S. Kirner, O. Gabriel, B. Stannowski, B. Rech and R. Schlatmann, *Applied Physics Letters*, 2013, 102, -.
50. S. Xu, X. Zhang, Y. Li, S. Xiong, X. Geng and Y. Zhao, *Thin Solid Films*, 2011, 520, 694-696.
51. T. Nishimoto, M. Takai, H. Miyahara, M. Kondo and A. Matsuda, *Journal of Non-Crystalline Solids*, 2002, 299-302, Part 2, 1116-1122.
52. I. Milosavljevic and E. M. Suuberg, *Industrial & Engineering Chemistry Research*, 1995, 34, 1081-1091.
53. NIST Standard Reference Data, <http://webbook.nist.gov/chemistry/mw-ser.html>.
54. I. Ferreira, V. Silva, H. Águas, E. Fortunato and R. Martins, *Applied Surface Science*, 2001, 184, 60-65.
55. R. Martins, L. Raniero, L. Pereira, D. Costa, H. Águas, S. Pereira, L. Silva, A. Goncalves, I. Ferreira and E. Fortunato, *Philosophical Magazine*, 2009, 89, 2699-2721.
56. V. V. Brazhkin and A. G. Lyapin, *Nat Mater*, 2004, 3, 497-500.
57. Y. Li and D. Du, *Characterization of Low Temperature Deposited Flexible Amorphous Silicon Solar Cells*, 2009.
58. J. K. Rath, M. Brinza and R. E. I. Schropp, in *2009 34th IEEE Photovoltaic Specialists Conference, Vols 1-3*, Ieee, New York, 2009, pp. 1743-1746.
59. R. F. P. Martins, A. Ahnood, N. Correia, L. M. N. P. Pereira, R. Barros, P. M. C. B. Barquinha, R. Costa, I. M. M. Ferreira, A. Nathan and E. E. M. C. Fortunato, *Advanced Functional Materials*, 2013, 23, 2153-2161.
60. M. Foti, C. Tringali, A. Battaglia, N. Sparta, S. Lombardo and C. Gerardi, *Solar Energy Materials and Solar Cells*, 2014, 130, 490-494.
61. L. Pereira, D. Gaspar, D. Guerin, A. Delattre, E. Fortunato and R. Martins, *Nanotechnology*, 2014, 25, 094007.
62. J. Kalowekamo and E. Baker, *Solar Energy*, 2009, 83, 1224-1231.
63. F. C. Krebs, T. Tromholt and M. Jorgensen, *Nanoscale*, 2010, 2, 873-886.
64. T. M. Brown, F. De Rossi, F. Di Giacomo, G. Mincuzzi, V. Zardetto, A. Reale and A. Di Carlo, *Journal of Materials Chemistry A*, 2014, 2, 10788-10817.
65. H. Águas, S. K. Ram, A. Araujo, D. Gaspar, A. Vicente, S. A. Filonovich, E. Fortunato, R. Martins and I. Ferreira, *Energy & Environmental Science*, 2011.
66. E. Fortunato, L. Pereira, H. Águas, I. Ferreira and R. Martins, *Proceedings of the IEEE*, 2005, 93, 1281-1286.
67. R. A. Street, *Hydrogenated Amorphous Silicon*, Cambridge University Press, 2005.
68. Enfucell SoftBattery, <http://www.enfucell.com/softbattery>.
69. S.-F. Leung, L. Gu, Q. Zhang, K.-H. Tsui, J.-M. Shieh, C.-H. Shen, T.-H. Hsiao, C.-H. Hsu, L. Lu, D. Li, Q. Lin and Z. Fan, *Sci. Rep.*, 2014, 4.
70. S. M. Garner, H. Mingqian, L. Po-Yuan, S. Chao-Feng, L. Chueh-Wen, H. Yen-Min, R. Hsu, D. Jau-Min, H. Je-Ping, C. Yi-Jen, J. J. ChiehLin, L. Xinghua, M. Sorensen, L. Jianfeng, P. Cimo and C. Kuo, *Display Technology, Journal of*, 2012, 8, 590-595.

-
71. M. Brinza, J. K. Rath and R. E. I. Schropp, *Solar Energy Materials and Solar Cells*, 2009, 93, 680-683.
72. A. L. Mourad, E. E. C. Garciaa, G. B. Vilela and F. Von Zuben, *Resour. Conserv. Recycl.*, 2008, 52, 678-689.
- 5 73. M. Grosso, L. Biganzoli and L. Rigamonti, *Resour. Conserv. Recycl.*, 2011, 55, 1178-1184.
74. .
75. J. M. Pearce and A. Lau, *ASME Solar 2002: International Solar Energy Conference*, 2002, 181-186.
- 10 76. Y. Peng, Z. Q. He, A. Diyaf, A. Ivaturi, Z. Zhang, C. J. Liang and J. I. B. Wilson, *Applied Physics Letters*, 2014, 104.
77. F. Sergej Alexandrovich, Á. Hugo, B. Tito, V. António, A. Andreia, G. Diana, V. Marcia, L. Joaquim, F. Elvira and M. Rodrigo, *Science and Technology of Advanced Materials*, 2012, 13, 045004.
- 15 78. R. Martins, L. Raniero, L. Pereira, D. Costa†, H. Águas, S. Pereira, L. Silva, A. Gonçalves, I. Ferreira and E. Fortunato, *Philosophical Magazine*, 2009, 89, 2699-2721.
79. M. J. Mendes, S. Morawiec, F. Simone, F. Priolo and I. Crupi, *Nanoscale*, 2014, 6, 4796-4805.
- 20 80. P. Barquinha, R. Martins, L. Pereira and E. Fortunato, *Transparent Oxide Electronics: From Materials to Devices*, Wiley, 2012.

25